Desalination and Water Treatment
www.deswater.com
doi: 10.5004/dwt.2019.24584

167 (2019) 245–257
November

Green synthesis of ZnO nanoparticles by *Coriandrum sativum* leaf extract: structural and optical properties

G. Yashni, A.A. Al-Gheethi*, R.M.S.R. Mohamed*, Amir Hashim M.K.

Department of Water and Environmental Engineering, Universiti Tun Hussein Onn Malaysia, 86400 Parit Raja, Batu Pahat, Johor Malaysia, Tel. +601111098362; Fax: +607-4536588; emails: adel@uthm.edu.my/adelalghithi@gmail.com (A.A. Al-Gheethi), maya@uthm.edu.my (R.M.S.R. Mohamed), yashni_g@yahoo.com (G. Yashni), amir@uthm.edu.my (Amir Hashim M.K.)

Received 25 February 2019; Accepted 16 June 2019

ABSTRACT

The study aims to synthesise zinc oxide nanoparticles (ZnO NPs) by green method using *Coriandrum sativum* leaf extract as a reduction and capping agent. ZnO NPs were calcined at two different temperatures (100°C and 550°C). The optical properties of ZnO NPs were characterised by UV–Vis spectrophotometer, while the structural properties were characterised by field emission scanning electron microscopy (FESEM) with energy dispersive X-ray spectroscopy (FESEM/EDX), transmission electron microscopy (TEM), X-ray diffraction (XRD), and Fourier transform infrared spectroscopy (FTIR). ZnO NPs solution exhibited high absorbance at 213–330 nm, while the maximum absorbance values of ZnO NPs (100°C) and ZnO NPs (550°C) in diffuse reflectance mode were at 333 and 348 nm, which correspond to band gap energy of 3.56 and 3.72 eV, respectively. FESEM images showed that ZnO NPs were clearly distinguished as individual particles with little agglomeration. The size of the particles of ZnO NPs (100°C) is in the range of 58.2 to 216 nm and in the range of 84.8 to 113 nm for ZnO NPs (550°C) as determined by TEM analysis. Moreover, the XRD patterns of ZnO NPs (100°C) and ZnO NPs (550°C) confirmed the hexagonal wurtzite structure with an average crystallite size of 60.85 and 55.13 nm, respectively. In contrast, FTIR revealed the characteristics of ZnO NPs (100°C) and ZnO NPs (550°C) vibrational modes at 500 and 600 cm^{-1}, respectively. FTIR spectra confirmed the presence of –C–O, =C–H, C=C, –C–O–C, O–H and amide I bond in both types of ZnO NPs. These findings indicate that *C. sativum* leaf extract is an effective reducing/stabilising agent for the green synthesis of ZnO NPs. However, ZnO NPs (550°C) exhibited better structural properties compared with ZnO NPs (100°C).

Keywords: Biosynthesis; Capping agent; Stabilising agent; Phytochemicals; Calcination

1. Introduction

Nanotechnology is one of the most promising modern technologies in various science fields such as environmental health, food, cosmetics, feed, and space No. 92. Nanoparticles (NPs) are particles with a dimension of 100 nm or less and have a large surface-area-to-volume ratio. NPs show better properties compared with their bulk counterparts in terms of crystal structure, chemical composition, surface area, surface energy, surface roughness, and physiochemical stability depending on their size, distribution, and morphology [1,2]. Zinc oxide (ZnO) has wide band gap of 3.2 eV and excitonic binding energy of 60 meV. It crystallises in the wurtzite structure [3]. ZnO NPs are getting much attention in various applications such as in biomedicine, optoelectronic and photonic devices, solar cells, and photocatalysts [4,5]. NPs can be synthesised by chemical, physical, or biological methods. However, the chemical and physical methods are expensive due to costly stabilising/reducing agent and equipment as well as having toxic byproducts. For instance, utilisation of highly reactive reducing agents such as sodium borohydride ($NaBH_4$) and hydrazine hydrate

* Corresponding authors.

(N_2H_4) can cause unwanted toxicity issues and the formation of toxic byproducts [6,7]. Therefore, green synthesis has been explored as an approach to synthesise metal NPs with controlled size and shape [8].Green synthesis utilises pollutant-free chemicals and solvents such as water and natural extracts to synthesise NPs [7]. The green method has no requirement of high temperature for synthesis and calcinations and can be easily scaled up. In comparison, ZnO NPs synthesised using emulsion chemical requires a calcination temperature of 700°C–1,000°C [9,10], and vapour transport method needs high temperatures such as ~1,400°C [11]. In addition, plant-mediated green synthesis has gained much attention due to the use of natural capping agents and the absence of toxic chemicals [12]. Green leaves are the most suitable materials to synthesise ZnO NPs as they are the site of photosynthesis and have more H^+ ions to reduce zinc acetate dehydrate (the precursor) into ZnO NPs [13]. Among several plant extracts, *Cassia fistula* [14], *Moringa oleifera* [15], *Laurus nobilis* [16], *Caralluma fimbriata* [17], *Vitis labrusca* [18], *Artocarpus heterophyllus* [19], *Aristolochia indica* [20], and *Carica papaya* [21] have been explored as natural reducing/capping agents for ZnO NPs synthesis. However, a little agglomeration was observed in the ZnO NPs produced from these plants, indicating the lesser effectiveness of these extracts as a reducing/capping agent. Therefore, in this study, *Coriandrum sativum* was explored as an alternative reducing/capping agent for the synthesis of ZnO NPs due to its abundance in phytochemicals.

Coriandrum sativum, also known as cilantro or Chinese parsley, is a widely available plant in tropical countries [22]. *C. sativum* contains phytochemicals such as flavonoids, terpenoids, phenols, alkaloids, carbohydrates, tannins, protein, gardiac glycosidase, and minerals. It also contains niacin, calcium, carotene, phosphorus, and iron, which are responsible for the synthesis of metal NPs [2]. For instance, phenolics have nucleophilic aromatic rings which have antioxidant potential and metal-chelating ability. Moreover, flavonoids are the most important bio-reducing agent of plant extracts because of their ability to donate electrons and hydrogen atoms. Similarly, proteins act as a reducing agent where they donate electrons to react with metal ions and their consequent stabilisation that indicates the nanoparticle formation [23]. *C. sativum* leaf extracts have been explored in the synthesis of silver nanoparticles [2,24–26] via oxidation or reduction reactions. However, less attention is paid for the synthesis of ZnO NPs from *C. sativum* plant extract. In this study, ZnO NPs were synthesised at two different temperatures (100°C and 550°C) to study the effects of calcination temperature on the optical and structural properties of ZnO NPs, since it has not been reported before.

The effect of calcination at 60°C on the properties of ZnO NPs synthesized from *C. sativum* has been investigated by researchers in the literature [7,26]. Moreover, ZnO NPs synthesized from *C. sativum* which was extracted by ethanol has been investigated by researchers in the literature [27]; meanwhile a study by Singh et al. [28] investigated the properties of ZnO NPs synthesized from powdered *C. sativum* where reaction with the precursor and *C. sativum* extract took place at 70°C. However, the phytochemical analysis of the *C. sativum* by GCMS used in the synthesis has not reported before. *C. sativum* has a complicated composition with high diversity of the chemical compounds, therefore, the phytochemical analysis is necessary to determine the main compounds involved in the formation of ZnO NPs. Moreover, the UV–Vis studies of *C. sativum* have not been reported by the previous studies. The investigation the UV–Vis absorption analysis of *C. sativum* leaf extract is needed to enhance the determination of the fingerprint signals shown by *C. sativum* leaf extract. The present study aimed to use *C. sativum* leaf extract as a reducing and capping agent for green synthesis of ZnO NPs with zinc acetate dihydrate ($ZnC_4H_6O_4$) as precursor where the reaction occurred at room temperature. ZnO NPs were characterised to determine its maximum absorbance, surface morphology, elemental composition, internal structure size, crystallographic structures and the possible functional groups in ZnO NPs. both phytochemical analysis as well as UV–Vis studies of *C. sativum* was studied which emphasise the novelty of the current work.

2. Materials and methods

2.1. Preparation of C. sativum extract

Fresh *C. sativum* leaves were collected from in and around the regions of Taman Universiti, Batu Pahat, Malaysia. The leaf were shredded and washed several times with distilled water to remove impurities and dust particles. Clean *C. sativum* leaves were air-dried at room temperature (25°C ± 2°C) to remove residual moisture. A fixed weight (50 g) of the washed and dried leaves was mixed with 200 mL (w/v) of deionised water in a 500 mL glass beaker. The mixture was stirred and boiled at 60°C for 30 min until the colour of the aqueous solution changed to dark yellow. The *C. sativum* extract was cooled to room temperature (25°C ± 2°C) and filtered using Whatman filter paper (No. 40) [2,26]. The filtrate was collected and the extract was stored in a glass bottle at 4°C for subsequent UV–Vis studies and phytochemical analysis of extract and for synthesis of ZnO NPs.

2.2. Synthesis of ZnO NPs

ZnO NPs was synthesised by adding 20 mL of 0.02 M zinc acetate dihydrate ($ZnC_4H_6O_4$) to 50 mL DW. The mixture was stirred using a magnetic stirrer (200 rpm) for 10 min. Thereafter, 1 mL of the aqueous leaf extract of *C. sativum* was added into the solution and the pH of the solution was adjusted to 12 by 2.0 M NaOH until a pale white aqueous solution formed. The mixture was stirred again (1,000 rpm) for 2 h until a white precipitate was formed. The white precipitate was separated by centrifugation (4,000 rpm) for 25 min. The precipitate was washed once with 5 mL of DW and 95% ethanol for 1 min to remove impurities. The precipitate was dried at 100°C in a drying oven (Binder, Germany) overnight to obtain pale white ZnO NPs powder. For the second type of ZnO NPs, the ZnO NPs are calcined at 550°C in a furnace (Protherm, Turkey) for 3 h after drying at 100°C to obtain ZnO NPs with high purity [27,28].

2.3. Characterisation of C. sativum leaf extract

The optical characteristics of *C. sativum* leaf extract were analysed with a UV–Vis absorption spectrophotometer, while the phytochemical properties were determined by using gas

chromatography–mass spectrometry (GCMS) as described in Sections 2.3.1 and 2.3.2, respectively.

2.3.1. UV–Vis absorption analysis of C. sativum leaf extract

The optical property of *C. sativum* leaf extract was analysed with a UV–Vis absorption spectrophotometer (DR6000) in the range of 190–1,100 nm to determine its fingerprint signals [21].

2.3.2. Phytochemical analysis of C. sativum leaf extract

Phytochemical compounds of *C. sativum* leaf extract was determined using GCMS using a thermal separation probe (GCMS [TSP]) (Agilent Technologies 7890B [GC], Central laboratory, Universiti Malaysia Pahang) equipped with an Agilent 5977A mass selective detector. *C. sativum* leaf extract was freeze-dried at −70°C overnight. The sample was placed inside an Agilent ultra inert glass microvial and inserted into the TSP. The samples were placed through thermal desorption by inserting the probe into a TSP adapter [28]. The injector and detector temperatures were set at 250°C and 290°C, respectively. The column temperature was initially programmed at 50°C for 5 min, followed by an increase of 5°C/min to 270°C, and maintained isothermally for 10 min. One microlitre of sample was injected to HP-5MS (5% phenyl methyl siloxane) capillary column of dimensions 30 m × 250 μm × 0.25 μm. The carrier gas was helium with a flowrate of 1 mL min^{-1}. The MS was operated at 70 eV, full scan in EI mode (40–600 amu), transfer line temperature of 270°C, and ion source temperature of 200°C. The identification of the compounds present in the *C. sativum* leaf extract was compared with the NIST library [21,29].

2.4. Characterisation of ZnO nanoparticles

The optical properties of ZnO NPs were characterised by UV–Vis absorption spectrophotometer (DR6000) as described in Section 2.4.1, while the structural properties were characterised by field emission scanning electron microscopy (FESEM) with energy dispersive X-ray spectroscopy (FESEM/EDX) (Section 2.4.2), transmission electron microscopy (TEM) (Section 2.4.3), X-ray diffraction (XRD) (Section 2.4.4), and Fourier transform infrared spectroscopy (FTIR) (Section 2.4.5).

2.4.1. UV–Vis spectroscopy analysis

The optical property of ZnO NPs solution was analysed via a UV–Vis absorption spectrophotometer (DR6000) in the range of 190–1,100 nm [21]. The absorbance of ZnO NPs powder was measured by a UV–visible near-infrared (UV–Vis NIR) spectrophotometer (Shimadzu-Model UV-2600, Micropollutant research centre (MPRC)) with the wavelength ranging from 200 to 1,000 nm in the diffuse reflectance mode to determine its band gap energy [30].

2.4.2. Field emission scanning electron microscopy and energy dispersive X-ray (FESEM/EDX)

The surface morphology and elemental composition of both types of ZnO NPs were analysed by FESEM/EDX [31]. The sample was prepared by mixing two drops of 100% ethanol with 1 g ZnO NPs on clean silicon wafers, and then dried at 60°C for 2 min to completely eliminate the solvent [16,32]. FESEM images and EDX spectra of the samples were obtained using field electron microscopy and Ion Company, United States (FEI) (Quanta 450) equipped with an energy dispersive X-ray analyser at an accelerating voltage of 20 kV.

2.4.3. Transmission electron microscopy analysis

The internal structure and size of ZnO NPs were determined by using FEI (TECNAI G2 20 TWIN [200 kV]) [33]. A fixed weight (0.9 g) of ZnO NPs was added in a 1.75 mL clear neutral wide mouth glass vial followed by the addition of 1 mL 95% ethanol. The vial was closed, sealed, and labelled, and then sonicated for 1 h. After sonication, the vial was opened and a single droplet of the sonicated liquid sample was dropped onto a Formvar carbon-coated grid using a dropper. The droplet was air-dried, leaving only the solid nanoparticles on it. The grid was then transferred onto a sample holder for TEM observation [32].

2.4.4. X-ray diffraction analysis

XRD was conducted to get detailed information about the chemical composition and crystallographic structures of ZnO NPs [25]. XRD analysis of ZnO NPs was performed using a RIGAKU (Central laboratory, Universiti Malaysia Pahang), Miniflex II. Cu radiation (λ = 1.540598 Å). 1 g of ZnO NPs was spread in the holder ring and pressed using the powder press block. ZnO NPs that flowed out during pressing was scraped using the knife blade. Excess ZnO NPs above the rim of the holder ring was removed using the knife blade and dusting brush. The bottom plate was placed onto the holder ring and clamped in position gently to prevent the ZnO NPs from becoming loose or damaged. The sample holder was removed from the preparation table by turning it upside down and pressing the spring-loaded knob. Then, the ZnO NPs were analysed using High Score Plus software with measuring parameters of 40 kV, 30 mA with a rate of 2°/min and run at the 2θ range (10°–80°) with a step size of 0.05.

2.4.5. Fourier transform infrared spectra

Fourier transform infrared (FTIR) spectroscopy was used to detect the possible functional groups in ZnO NPs. The ZnO NPs were characterised using Nicolet iS50 (Thermo Scientific, United States) at a scanning range of 400–4,000 cm^{-1} using attenuated total reflection (ATR) method. First, the crystal plate (sample holder) was cleaned with acetone. 5 mg of sample was placed directly on the crystal plate and then pressed using the metallic pressing device. Lastly, the sample was scanned to get the IR spectrum [8].

3. Results and discussion

3.1. Characterisation of C. sativum leaf extract

The results of *C. sativum* leaf extract analysis by UV–Vis absorption spectrophotometer (DR6000) and GCMS analysis is described in Sections 3.1.1 and 3.1.2, respectively.

3.1.1. UV–Vis studies of C. sativum leaf extract

The absorption spectrum of *C. sativum* extract by using UV–Vis spectrophotometry extract is shown in Fig. 1. The fingerprint signals appeared at around 404 nm (bond I) and 332 nm (bond II) which are attributed to the cinnamoyl and benzoyl systems of the flavonoid nuclei, respectively. This is due to the $\pi \rightarrow \pi^*$ transitions of conjugated double bonds of the flavone nucleus [6,34]. Hence, the results prove the presence of flavonoid in the *C. sativum* extract. Besides that, beta-carotene (a type of terpenoid) absorbs strongly in the visible region between 400 and 500 nm. The strong absorption at 404 nm proves the presence of terpenoids in *C. sativum* extract. In comparison, the fingerprint signals of *Euphorbia prolifera* extract were at 320 (bond I) and 247 nm (bond II) [34], *Hippophae rhamnoides* at 285 and 245 nm [35], and *Euphorbia heterophylla* at 360 and 250 nm [36]. The absorption spectrum of *C. sativum* extract exhibited higher fingerprint signals compared with previous studies. This proves that *C. sativum* leaf extract works better with ultraviolet (UV, 190–400 nm) and visible (VIS, 400–800 nm) regions since the fingerprint signals appeared around 332 and 404 nm.

3.1.2. Phytochemical properties of C. sativum leaf extract

The phytochemical properties *C. sativum* leaf extract as determined by GCMS is illustrated in Table 1. Forty-three compounds were recognised, in which the highest composition peaks were determined for 1(2H)-naphthalenone and 2-anilino-4-methylquinoline (18.67%), isocoumarin-3-one, 4,4,5,6,8-pentamethyl- and 6-methyl-2-oxo-1,2-dihydro-3,4-pyridinedicarbonitrile (17.17%), d-alloisoleucine and acetamide, *N*-methyl-*N*-(2-phenylethyl) (14.34%), 2,1,3-benzothiadiazole, 2,3,5-trimethyl methylcarbamate, and 3,5-dime thylanisole (8.32%), benzoic acid, 4-amino-2-chloro-, -(diethylamino)ethyl ester and l-leucyl-p-nitroanilide (6.25%), ethyl diphenylphosphinite and hexahydrofluorene, 3-methoxy-6-methyl (5.89%), 2-methoxy-4-vinylphenol and 4-hydroxy-3-methylacetophenone (3.98%) and 3-methyl-4-phenyl-1H-pyrrole, quinoline, 8-ethyl and 1,2,3,4-tetrahydro-cyclopenta[b]indole (2.95%), which represent the phytochemicals of terpenoids, flavonoids, alkaloids, proteins, phenols, minerals, and quinone, respectively. These bioactive phytochemical constituents act as a key factor for the reduction of Zn ions to ZnO NPs and they are responsible for the potent antibacterial, antioxidant, and anticancer bioactivities enhanced by ZnO NPs derived from *C. sativum* leaf extract [29]. It has been suggested that the phytochemicals are involved directly in the reduction of the ions and formation of NPs, even though the mechanism involved in each plant is different as the phytochemicals in each plant vary [13].

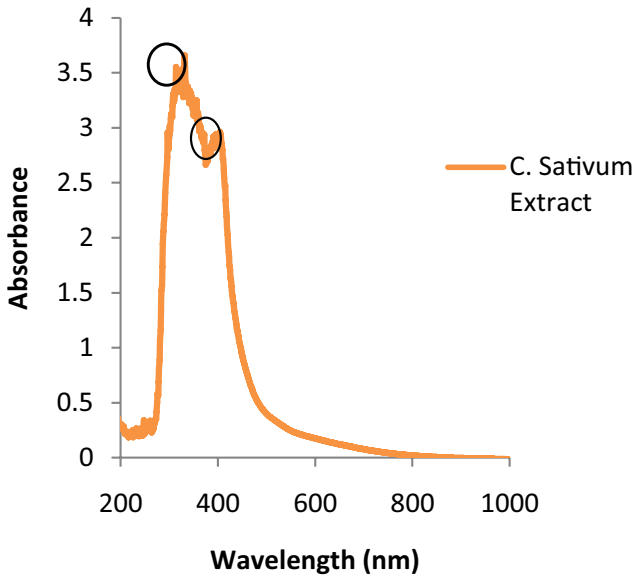

Fig. 1. Absorption spectrum of *Coriandrum sativum* extract.

3.2. Characterisation of ZnO NPs synthesised from leaf extract of C. sativum

3.2.1. UV–Vis properties of ZnO NPs

The UV–Vis properties of ZnO NPs are depicted in Fig. 2, which shows the changes in the *C. sativum* leaf extract colour from dark yellow to pale white after the addition of NaOH and to white after 2 h of stirring. These changes might be due to the excitation of surface plasmon vibrations with the ZnO NPs [12]. The changes in the colour confirmed the completion of reaction between *C. sativum* leaf extract and zinc acetate dihydrate, forming ZnO NPs. The surface plasmon absorption takes place due to the collective oscillation of the free conduction band electrons which are excited by the incident electromagnetic radiation and occurs as the diameter of particles is smaller than the wavelength of incident light [37]. The formation of ZnO NPs was confirmed using a spectrophotometer (Fig. 3), which showed that the ZnO NPs exhibited high absorbance detected at 304, 293, 325, 329, 325, 323, 330, and 213 nm after 1, 2, 3, 4, 5, 6, 7, and 30 d, respectively, due to the surface plasmon absorption of ZnO NPs which lies between the band gap wavelength of 333 and 348 nm (E_g = 3.72 and 3.56 eV), respectively [38]. The absorption spectrum of ZnO NPs is an indication of ZnO excitation by UV and visible light [26]. The presence of band between 213 and 330 nm is an indication of nanoparticle formation. The maximum absorbance of ZnO NPs synthesised from leaf extract of *Buchanania lanzan* was between 360 and 377 nm [37] and between 371 and 376 nm for ZnO NPs prepared by using *Azadirachta indica* [39]. Meanwhile, Suresh et al. [40] observed an absorption peak at 370 nm for ZnO NPs synthesised from *Pongamia pinnata* leaf extract and Nagajyothi et al. [41] observed a strong UV absorption from 360 to 370 nm for ZnO NPs synthesised from *Plectranthus amboinicus* leaf extract. The shift of absorption edge to the lower wavelength or higher energy indicates a decrease in the NPs size [42]. These findings prove that the green synthesised ZnO NPs solution remained stable even after 30 d of reaction completion. Moreover, the sharp absorption of ZnO NPs shows that the nanoparticles are monodispersed [43]. The stability is not related to temperature, the absorbance was recorded over 30 d to determine whether there were any drastic changes in the absorbance over the period. However, there were no drastic changes in absorbance where it remained in the range of temperature, which proves the stability of the ZnO NPs solution.

Table 1
GC–MS analysis report for the extract of *C. sativum* leaves extract

Peak No	Retention time (min)	Compound name	Molecular formula	Molecular weight (g/mol)	Peak area (%)
1	4.486	Butyrolactone, ethanamine, N-(ethoxymethyl)-N-ethyl	$C_4H_6O_2$, C_2H_7N, $C_7H_{17}NO$	86.09, 46.078, 131.219	0.33
2	5.676	Pyrazine, trimethyl-, 3-butyl-2,5-dimethyl	$C_7H_{10}N_2$, $C_{10}H_{16}N_2$	122.171, 164.252	0.28
3	6.211	3(2H)-Isothiazolone, 2-methyl-, 2-butenediamide, (E)-, glutaric acid, hexyl octyl ester	C_4H_5NOS, $C_4H_6N_2O_2$ $C_{18}H_{34}O_4$	115.15, 114.104, 314.466	0.22
4	7.063	Taurultam, taurolidine, N-nitroso-2-methyl-oxazolidine	$C_3H_8N_2O_2S$, $C_7H_{16}N_4O_4S_2$, $C_4H_8N_2O_2$	136.169, 284.349, 116.12	0.15
5	8.494	4H-Pyran-4-one, 2,3-dihydro-3,5-dihydroxy-6-methyl-	$C_6H_8O_4$	144.126	1.39
6	8.793	4H-Pyran-4-one, 2,3-dihydro-3,5-dihydroxy-6-methyl-, Heptane, 2-6-dimethyl	$C_6H_8O_4$ C_9H_{20}	144.126 128.259	0.32
7	10.047	Benzofuran, 2,3-dihydro, benzeneethanamine, N-(3-chloropropyl)-alpha-methyl-, benzene, 1-ethynyl-4-fluoro	C_8H_8O $C_{12}H_{18}ClN$ C_8H_5F	120.151, 211.733, 120.126	0.86
8	10.511	Tridecane	$C_{13}H_{28}$	184.367	0.30
9	10.925	Thiophene-2-sulfonamide, N-(4-methoxyphenyl)-5-(2-pyridyl)-, pyridine-3-sulfonamide, 2-chloro-N-(4-methoxyphenyl)-4,6-dimethyl-, pyrazine, 3,5-dimethyl-2-propyl-	$C_{14}H_{15}N_3OS_2$ $C_{13}H_{13}ClN_2O_3S$ $C_9H_{14}N_2$	305.414 312.76 150.225	0.18
10	11.033	2-Methoxy-4-vinylphenol, 4-hydroxy-3methylacetophenone	$C_9H_{10}O_2$	150.177	3.98
11	11.574	Naphthalene,1,2-dihydro-1,5,8-trimethyl-, 1,1,5-trimethyl-1,2-dihydronaphthalene	$C_{13}H_{16}$	172.271	0.19
12	12.153	2-Propenethioamide, 3-(acetyloxy)-N,N dimethyl-, (E)-, N-Acetylmannosamine 1-Propanamine, N-nitro	$C_7H_{11}NO_2S$, $C_8H_{15}NO_6$, C3H8N2O2	173.23 221.209 104.1078	2.41
13	12.388	N,N-Dimethylacetoacetamide, propanamide 2-methyl-	$C_6H_{11}NO_2$, C_4H_9NO	129.159 87.1204	0.12
14	14.036	2,1,3-Benzothiadiazole, 2,3,5-trimethyl methylcarbamate, 3,5-dimethylanisole	$C_6H_4N_2S$ $C_{11}H_{15}NO_2$ $C_9H_{12}O$	136.172 193.246 136.194	8.32
15	14.577	Bis-[(formyl-methyl-amino)-methyl-phosphinic acid, 3,5-dihydroxycyclohexanamine, Ethanol, 2-(butylamino)-	$C_6H_{13}N_2O_4P$ $C_6H_{13}NO_2$ $C_6H_{15}NO$	208.152 131.173 117.192	0.36
16	14.863	D-Leucine, ethanol, 2-(butylamino)-	$C_6H_{13}NO_2$ $C_6H_{15}NO$	117.192 131.175	0.39
17	14.984	Bis-[(formyl-methyl-amino)-methyl]-phosphinic acid, D-leucine, 1-pentanamine, N-methyl-N-(1-methylethyl)-	$C_6H_{13}N_2O_4P$ $C_6H_{13}NO_2$ $C_9H_{21}N$	208.152 117.192 143.274	0.80
18	15.276	3-Methyl-4-phenyl-1H-pyrrole, quinoline, 8-ethyl, 1,2,3,4-tetrahydro-cyclopenta[b]indole	$C_{12}H_{11}NO_2$ $C_{12}H_{11}NO_2$ $C_{11}H_{11}N$	201.225 201.225 157.216	2.95
19	15.601	Acetamide, N-[2-(4-bromophenoxy)ethyl], 2-(Pentylamino)ethanol, cis-4-hydroxy-L-proline	C_2H_5NO $C_7H_{17}NO$ $C_5H_9NO_3$	59.07 131.219 131.131	2.66
20	15.671	Ethane, 1-[(2-diethylamino)ethylthio]-2-[(2-diethylamino) ethyldithio]-, D-alloisoleucine, N,N-methylisopropyltryptamine	$C_6H_{15}NS$ $C_6H_{13}NO_2$ $C_{15}H_{22}N_2O$	133.253 131.175 246.354	1.78

(*Continued*)

Table 1 Continued

21	15.852	L-Leucyl-p-nitroanilide, D-alloisoleucine, tenamfetamine	$C_{12}H_{17}N_3O_3$ $C_6H_{13}NO_2$ $C_{10}H_{13}NO_2$	251.28 131.175 179.219	2.03
22	16.192	Benzoic acid, 4-amino-2-chloro-, -(diethylamino)ethyl ester, L-leucyl-p-nitroanilide, D-alloisoleucine	$C_{13}H_{20}Cl_2N_2O_2$ $C_{12}H_{17}N_3O_3$ $C_6H_{13}NO_2$	307.216 131.175 179.219	6.25
23	16.523	D-Alloisoleucine, acetamide, N-methyl-N-(2-phenylethyl)-, 3-Methoxy, 3-(methylamino)-2-propenoic acid, methyl ester	$C_6H_{13}NO_2$ $C_{11}H_{15}NO$ $C_6H_7NO_3$	131.175 177.247 141.126	14.34
24	16.975	beta.-Carboline, 8-methoxy-1-methyl-, 5-Cyano-1,2,3,4 -tetrahydro-6-methyl-2-oxo-4-phenylpyridine, beta.-Carboline, 6-methoxy-2-methyl-	$C_{13}H_{12}N_2O$ $C_{11}H_7N_3O_2$ $C_{12}H_{14}N_2O$	212.252 213.196 202.257	0.42
25	17.859	6-Methylquinolinic acid, Pth-threonine, 1,3-benzodioxole, 4-methoxy-6-(2-propenyl)-	$C_{11}H_9NO_2$ $C_{11}H_{12}N_2O_2S$ $C_{11}H_{12}O_3$	187.19466 236.289 192.2112	0.33
26	17.987	6-Methoxy-2,4-dihydroxy-1,5-naphthyridine, 6-hydroxy-9-[tetrahydro-2H-pyran-2-yl]-9H-purine, acetamide, N-isoxazolo[5,4-b]pyridin-3-yl-	$C_8H_6N_2O_2$ $C_{10}H_{12}N_4O_2$ $C_8H_6ClN_3O_2$	162.148 220.22788 211.61	0.38
27	20.245	2(1H)Naphthalenone, 3,4,4a,5,6,7,8,8a.alpha.-octahydro-5.alpha.-hydroxy-4a.alpha.,7,7-trimethyl-, acetate, 1,3-butanedione, 1-(4-methoxyphenyl)-, 2,5-dimethoxy-4-propoxy-beta-methyl-beta-nitrostyrene	C15H24 $C_{11}H_{12}O_3$ $C_{12}H_{15}NO_4$	204 192.214 237.255	0.99
28	20.875	Benzenamine, 2-methoxy-5-[5-(1H-pyrazol-1-yl)-1H-1,2,3,4-tetrazol-1-yl]-, 4-Methylesculetin, Benzoic acid, 4-pentyl-	$C_7H_6ClN_5$ $C_{10}H_8O_4$ $C_{12}H_{16}O_2$	195.61 192.17 192.258	1.55
29	21.168	Isocoumarin-3-one, 4,4,5,6,8-pentamethyl-, 6-methyl-2-oxo-1,2-dihydro-3,4-pyridinedicarbonitrile, naphthalene, 1,2,3,4-tetrahydro-1-methyl-8-(1-methylethyl)-	$C_{14}H_{16}O_3$ $C_{13}H_{10}N_2O$ $C_{15}H_{22}$	232.275 210.236 202.341	17.17
30	21.473	2,3-Hexadienoic acid, 2-methyl-4-phenyl-, ethyl ester, ethyl diphenylphosphinite, Hexahydrofluorene, 3-methoxy-6-methyl	$C_{15}H_{18}O_2$ $C_{14}H_{15}OP$ $C_{15}H_{20}O$	230.307 230.247 216.324	5.89
31	22.007	Furan-2-carboxylic acid, 5-(1-hexynyl)-, 2(1H) Naphthalenone, 3,4,4a,5,6,7,8,8a.alpha-octahydro-5beta-hydroxy 4a alpha, 7,7-trimethyl-, acetate	$C_{11}H_{12}O_3$ $C_{15}H_{24}$	192.214 204	0.14
32	23.413	2-Propenoic acid, 2-cyano-3(3methoxyphenyl)-, ethyl ester, 2,6-Diphenylpyridine, Benzylidine-.beta.-naphthylamine	$C_{13}H_{13}NO_3$ $C_{17}H_{13}N$ $C_{17}H_{13}N$	231.251 231.298 231.298	0.40
33	24.533	Benzamide, 2,4-dichloro-N-(2,6-dimethyl-4-nitrophenyl)-, 2,5-2,4-Dichloro-N-methylbenzamide	$C_8H_9NO_3$ $C_8H_7Cl_2NO$	167.164 204.05	0.56
34	24.673	Propiconazole, butyl 2,4-dichlorobenzoate, Benzoyl chloride, 2,4-dichloro-	$C_{15}H_{17}Cl_2N_3O_2$ $C_{11}H_{12}Cl_2O_2$ $C_7H_3Cl_3O$	342.22 247.118 209.45	0.43
35	25.449	6-Cyano-2-[p-cyanostyryl]pyridine, acetamide, 2-[2-(2-thienyl)-3-indolyl]thio-N-(2-hydroxyethyl)-, dibenzo[a,e]cyclooctene	$C_8H_8N_2O$ $C_{16}H_{12}$	148.165 204.272	0.99

(*Continued*)

Table 1 Continued

36	25.589	Indolizine, 7-methyl-, Indolizine, 5-methyl-, 5-(4-Isobutoxyphenyl)hydantoin	$C_{15}H_{13}N$ C_9H_9N $C_{24}H_{36}N_4O_5$	207.276 131.178 460.575	0.25
37	25.793	2,4(1H,3H)-Pyrimidinedione, 6-amino-1,3-di-2-propenyl-, 2-heptadecenal, E-14-hexadecenal	$C_{10}H_{13}N_3O_2$ $C_{17}H_{32}O$ $C_{16}H_{30}O$	207.229 252.442 238.415	0.31
38	25.952	2(1H)-Naphthalenone, 3,4,4a,5,6,7,8,8a.alpha-octahydro-5beta-hydroxy-4a alpha, 7,7-trimethyl-, acetate, 2,8-Dimethyl-2,3,4,5,6,7-hexahydro-1H-2-benzazonine, 4-pyridazinecarbonitrile, 3-amino-5-(4-chlorophenyl)-	$C_{11}H_{16}O$ $C_{14}H_{21}N$ $C_{11}H_7BrN_4$	164 203.323 275.109	0.25
39	26.690	1(2H)-Naphthalenone, 3,4-dihydro-2-(phenylmethylene)-, 2-anilino-4-methylquinoline	$C_{17}H_{14}O$, $C_{16}H_{14}N_2$	234.298 234.296	18.67
40	27.708	2(1H)-Naphthalenone, 3,4,4a,5,6,7,8,8a alpha-octahydro-5 beta-hydroxy-4a alpha,7,7-trimethyl-, acetate, 3-amino-4-(methylthio)benzotrifluoride	$C_{11}H_{16}O$ $C_8H_8F_3NS$	164 207.214	0.22
41	28.153	1-Methyl-3-[4-(1-trimethylsilyloxy ethylidene)-cyclohexa-3,5-dienylidene]-triazene, benz[e] azulene-3,8-dione, 5-[(acet yloxy)methyl]-3a,4,6a,7,9,10,10a,10b-octahydro-3a,10a-dihydroxy-2,10-dimethyl-, (3a alpha.,6a alpha,10 beta,10a beta.,10b beta)-(+)-2-butenenitrile, 2-chloro-3-(4 methoxyphenyl	$C_{22}H_{24}O_4$ $C_{11}H_{10}ClNO$	352.43 207.657	0.12
42	29.489	4-Allyl-5-furan-2-yl-2,4-dihydro-[1,2,4]triazole-3-thione, cyclopenteno[4.3-b]tetrahydrofuran, 3-[(4-methyl-5-oxo-3-phenylthio)tetrahydrofuran-2-yloxymethylene]-, Octasiloxane, 1,1,3,3,5,5,7,7,9,9,11,11,13,13,15,15-hexadecamethyl-	$C_9H_9N_3OS$ $C_{19}H_{18}O_5S$ $C_{16}H_{48}O_7Si_8$	207.251 358.408 577.23212	0.08
43	29.996	Adamantane-1-(3,3-dichloropropyn-1-yl), 1,4,7,10,13,16-Hexaoxanonadecane, 18-propyl-, 2,5,8,11,14-Pentaoxahexadecan-16-	$C_{13}H_{16}Cl_2$ $C_{16}H_{32}O_6$ $C_{11}H_{24}O_6$	243.171 320.426 252.305	0.24

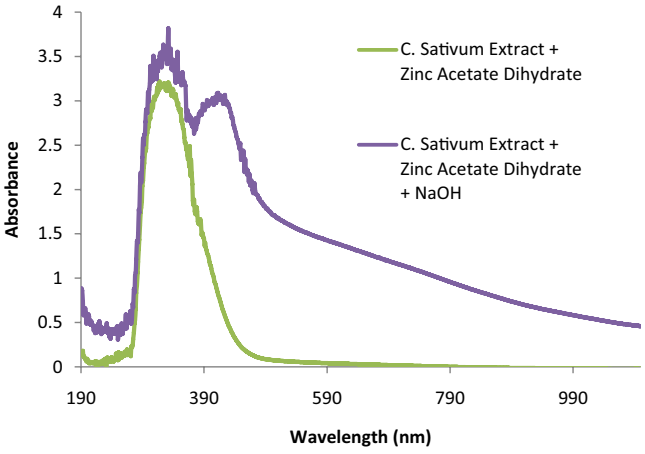

Fig. 2. Absorption spectrum during ZnO NPs synthesis.

3.3. Band gap measurement of ZnO NPs

The band gap energy (E_g) of ZnO NPs synthesised from *C. sativum* leaf extract was calculated from the intersection point of the vertical and horizontal part of the wavelength spectrum value as shown in Fig. 4 using the following equation:

$$E_g = \frac{hc}{\lambda}\text{eV}; \frac{1240}{\lambda}\text{eV} \quad (1)$$

The band gap energy was calculated by the above equation, where h is the Planck's constant (6.626×10^{-34} J s), C is the light velocity (3×10^8 m/s), and λ is the wavelength (nm) [44]. The maximum absorbance was observed at 333 nm for ZnO NPs (100°C) and 348 nm for ZnO NPs (550°C), which corresponded to band gap of 3.72 and 3.56 eV, respectively. The value is in good agreement with the band gap of ZnO NPs. These findings indicate that the increase in the calcination temperature caused an increase in ZnO NPs absorbance by decreasing the particle size [45]. Hence, the calcination temperature affects the particle size, which supports the results observed in the current study. This is because the removal of lattice water during the calcination process has a great potential to reduce the size of the ZnO NPs. The results are consistent with previous studies which revealed that the band gap of ZnO NPs synthesised from *Carica papaya* was 3.49 eV [22] and 3.32 eV from *Nephelium lappaceum* L. [26].

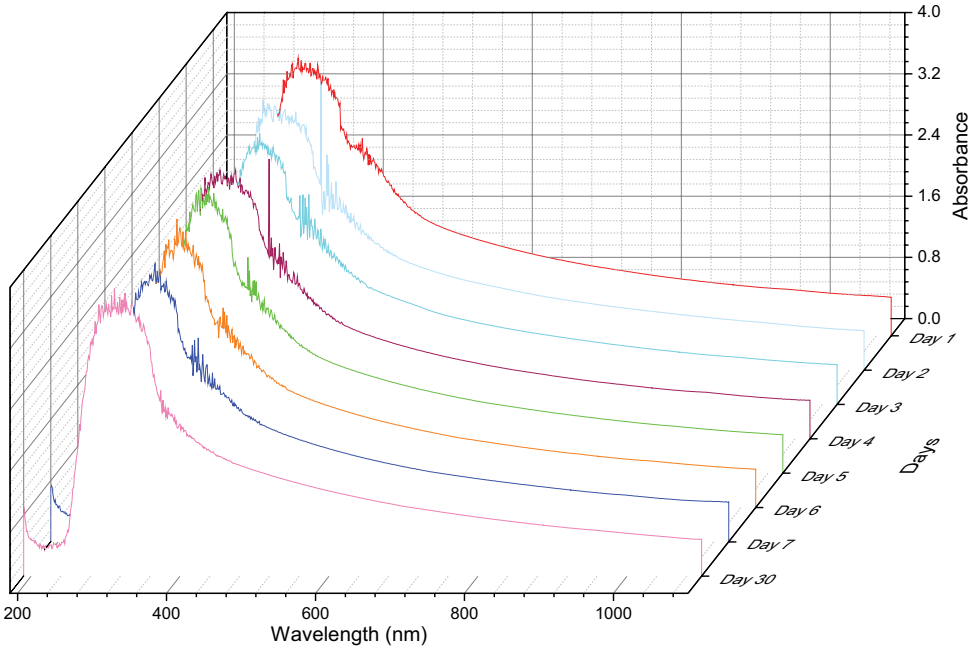

Fig. 3. Optical absorption spectrum of ZnO dispersed in water.

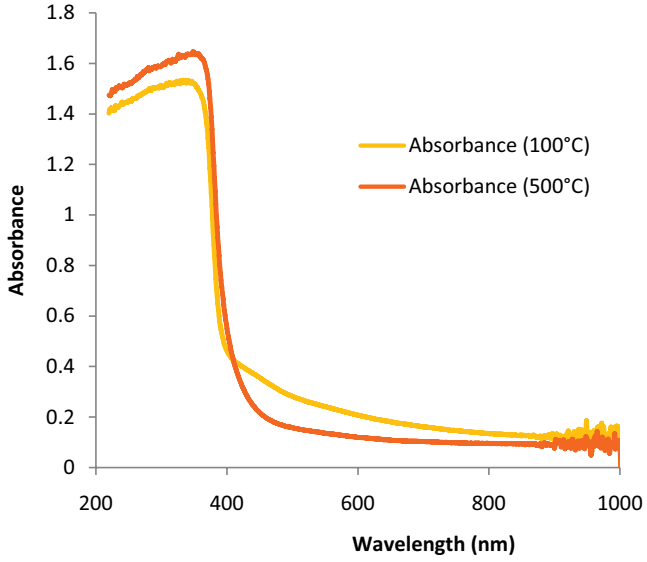

Fig. 4. Absorbance of ZnO NPs (powder).

These differences in the value for the band gap energy might be related to the differences in the type and amount of phytochemicals from different plant extracts.

3.4. Field emission scanning electron microscopy and energy dispersive X-ray analysis

The external morphology of ZnO NPs (100°C) and ZnO NPs (550°C) prepared with leaf extract of *C. sativum* is presented in Figs. 5a and b. The images revealed the formation of a hexagonal rod-like structure for ZnO NPs (100°C) and a spherical bead-like structure for ZnO NPs (550°C) with non-uniform distribution. These findings are consistent with the literature [46]. ZnO NPs synthesised from *Pongamia pinnata* leaf extract are mostly spherical [47,48] observed that the. Meanwhile, Karthik et al. [48] observed the shape of ZnO NPs synthesised from *Pongamia pinnata* extract to be spherical. In this study, both types of ZnO NPs were clearly distinguished as individual particles, which indicates the stabilisation of the ZnO NPs by the capping agent present in *C. sativum* leaf extract. Sundrarajan et al. [49] showed the FESEM images as individual and aggregate of particles. The study mentioned that the aggregation is due to the high surface energy of the particles. This indicates the effectiveness of *C. sativum* leaf extract as an efficient capping agent compared with other plant extracts. Moreover, ZnO NPs synthesised at the lower temperature (100°C) have a bigger size compared with those prepared at 550°C, indicating the role of calcination temperature in producing nanoparticles. These findings are consistent with those reported by Malaikozhundan and Vinodhini [43], who mentioned that the removal of lattice water during calcination has the ability to enhance NPs features. It can be concluded that the current study showed better FESEM results with less agglomeration of NPs as *C. sativum* leaf extract is an excellent capping and stabilising agent.

The EDX results of ZnO NPs composition are depicted in Figs. 6a and b. EDX pattern confirmed the presence of chemical constituents for ZnO NPs (100°C), where the weight percentages were Zn = 67.67% and O = 22.5% and the atomic percentages were Zn = 41.55% and O = 56.44%. Meanwhile, for ZnO NPs (550°C), the weight percentages were Zn = 81.11% and O = 18.89% and the atomic percentages were Zn = 51.24% and O = 48.76%. The presence of signal for gold in the EDX spectra is due to the gold-coating process for SEM analysis. No other significant components were detected, indicating the high purity of ZnO NPs. The strong intensity and narrow

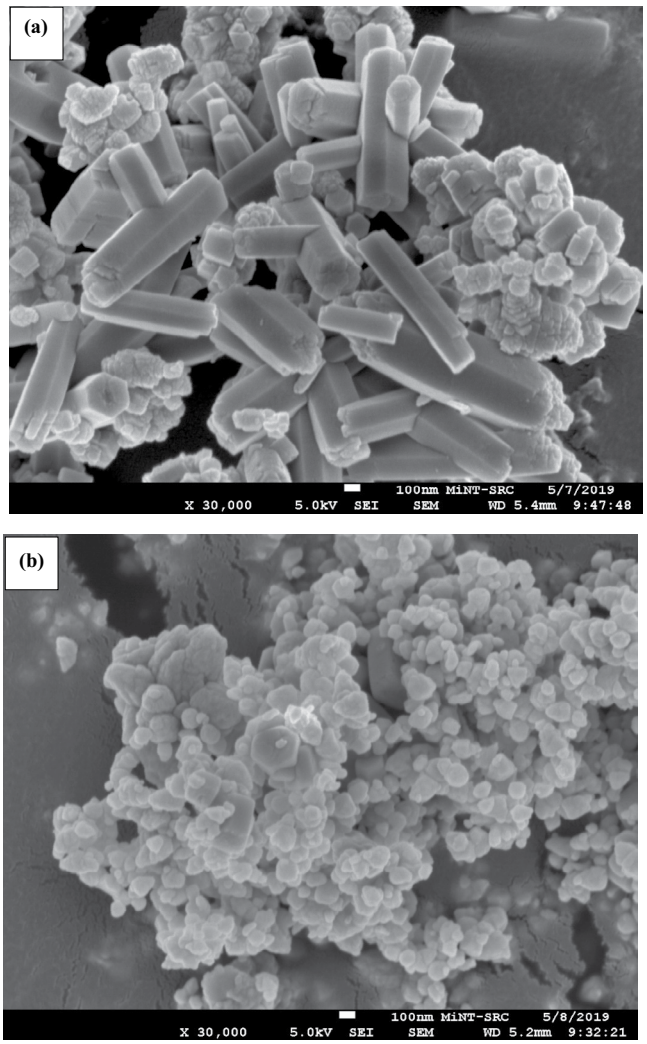

Fig. 5. FESEM images of external morphology ZnO NPs; (a) 100°C, and (b)550°C.

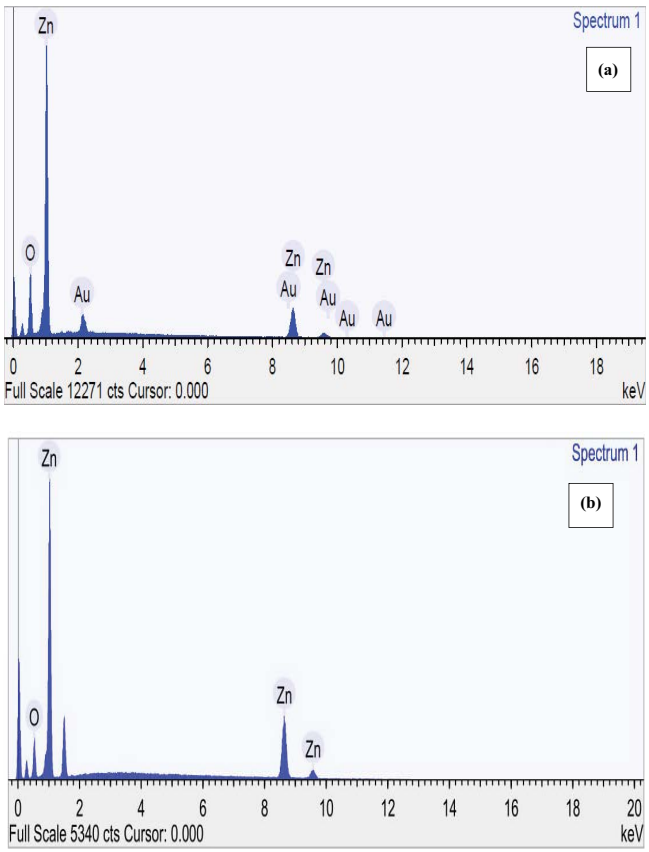

Fig. 6. (a) EDX spectra of ZnO NPs (100°C) and (b) EDX spectra of ZnO NPs (550°C).

width of ZnO diffraction peaks indicate that the ZnO were highly crystalline in nature [25]. These findings are in close agreement with a previous report [50] but with a slight difference due to variations in the chemical composition of ZnO NPs.

3.5. Transmission electron microscopy analysis

TEM was performed for ZnO NPs (100°C) and ZnO NPs (550°C) to determine the crystalline characteristics and size of the NPs. ZnO NPs (100°C) were hexagonal and the diameter ranged from 58.2 to 216 nm (Figs. 7a and b). In contrast, ZnO NPs (550°C) were quasi-spherical and hexagonal and the diameter was between 79.9 and 144 nm (Figs. 8a and b). Both types of ZnO NPs were transparent, which indicates that they are thin. However, thick nanoparticles were also noticed as two to three nanoparticles were overlying. The average particle size decreased as the calcination temperature increased. Both types ZnO NPs were enclosed by a thin layer of some capping of organic material from the *C. sativum* leaf extract. NPs showed individual dispersion with weak agglomeration. This might be due to the high surface energy of particles which attributed when the synthesis was performed in an aqueous medium or densification, resulting in narrow space between particles [29]. ZnO NPs synthesised from *Ulva lactuca* extract exhibited sponge-like asymmetrical shape and consisted of agglomerated NPs with an average size of 10–50 nm [51]. However, Sai-Saraswathi et al. [46] observed a spherical morphology with estimated average particle size of 40 nm. Momeni et al. [37] observed that the ZnO NPs synthesised from *Buchanania lanzan* agglomerated to form a foam-like bunch of particles while Geetha et al. [52] obtained quasi-spherical agglomerated NPs. In the present study, the *C. sativum* leaf extract acted as a better capping agent, forming ZnO NPs with well-defined quasi-spherical and hexagonal particles and with less agglomeration compared with previous research as can be observed from the TEM images.

3.6. X-ray diffraction analysis

XRD was used to analyse the composition and the phase purity of the ZnO NPs synthesised using *C. sativum* extract. XRD diffraction patterns of ZnO NPs (100°C) and ZnO NPs (550°C) are presented in Figs. 9a and b. ZnO NPs (100°C) had high diffraction peak with 2θ values at 31.79°, 34.43°, 36.28°, 47.57°, 56.62°, 62.88°, 66.42°, 67.96°, 69.10°, 72.56°, and 76.96°, corresponding to the crystal planes (h,l,k) of (010), (002), (001), (012), (110), (013), (020), (112), (021), (004),

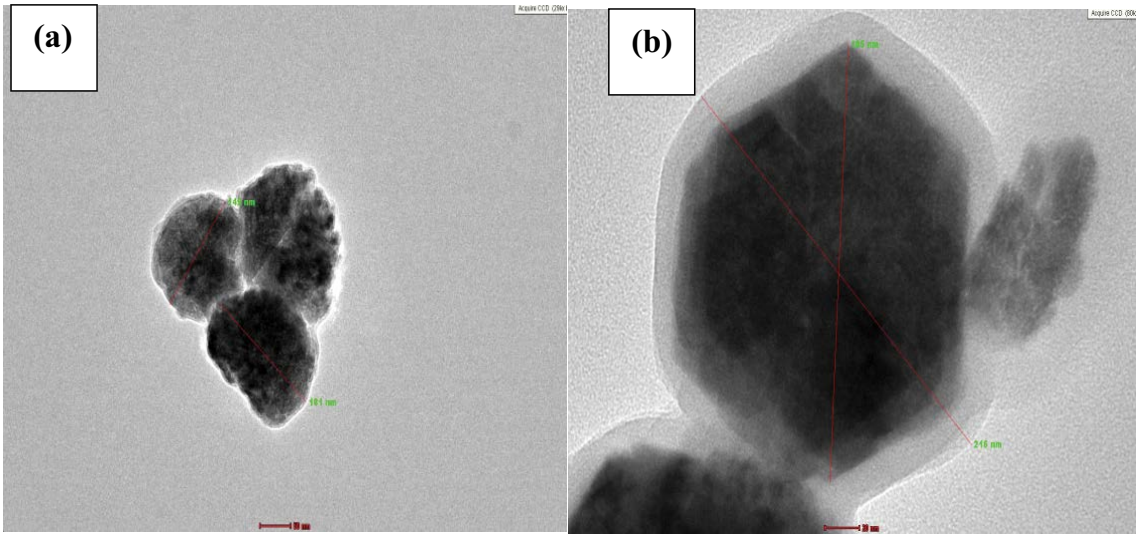

Fig. 7. (a,b) TEM image of internal structure and size of ZnO NPs (100°C).

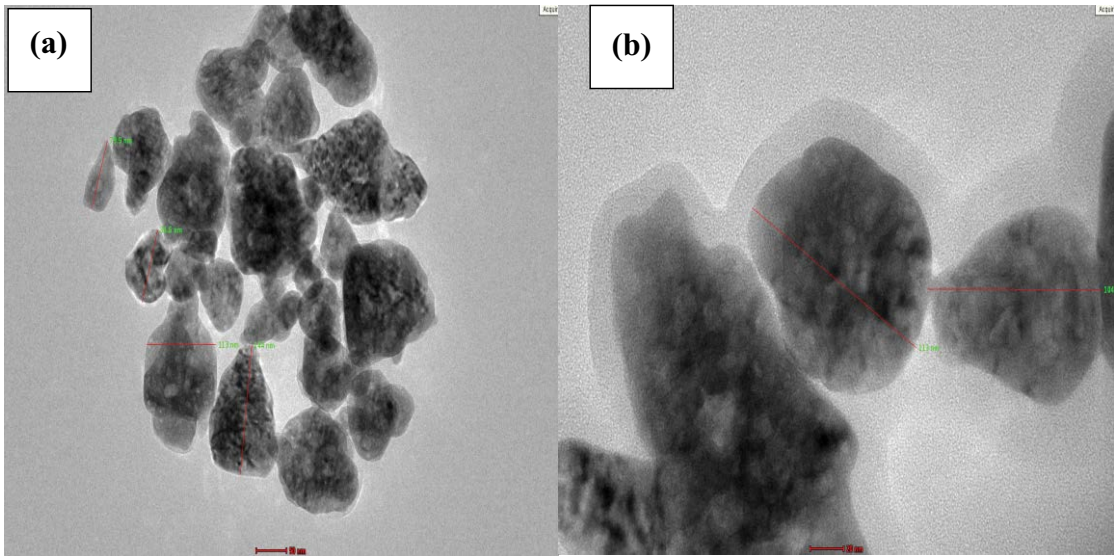

Fig. 8. (a,b) TEM image of internal structure and size of ZnO NPs (550°C)

and (022), respectively. ZnO NPs (550°C) exhibited high diffraction peak with 2θ values observed at 31.75°, 34.41°, 36.24°, 47.54°, 56.59°, 62.86°, 66.37°, 67.95°, 69.10°, 72.57°, and 76.96°, corresponding to the crystal planes (h,l,k) of (010), (002), (001), (012), (110), (013), (020), (112), (021), (004), and (022). The (011) diffraction peak in the XRD of ZnO NPs (100°C) and ZnO NPs (550°C) is more intense compared with (010) and (002) peaks, which indicates that the preferential growth of NPs is in the (011) crystallographic plane. Sundrarajan et al. [49] observed that the diffraction peaks of ZnO NPs synthesised from leaf extract of *Artocarpus heterophyllus* are positioned at 31.74°, 34.38°, 36.30°, 47.51°, 56.61°, 62.81°, 66.36°, 68.98°, and 69.10° that can be indexed to the (100), (002), (101), (102), (110), (103), (200), (112), and (201) planes of ZnO, respectively. Furthermore, Vijayakumar et al. [16] and Ishwarya et al. [53] showed the diffraction peaks of ZnO NPs synthesised from *Musa paradisiaca* and *Laurus nobilis* leaf extract at (100), (002), (101), (102), (110), (103), (200), (112), (201), (004), and (202). In a study by Prachayasittikul et al. [22], ZnO NPs synthesised using *Carica papaya* seed extract have (101) compared with (100) and (002) peaks growth of NPs is in the (101) crystallographic plane. The sharp diffraction peaks in the XRD pattern distinctly depict the crystalline nature of the sample [54]. The diffraction peaks represent the crystal structure of ZnO, which is hexagonal wurtzite according to standard JCPDS data card (JCPDS Card No: 00-001-1136) with lattice parameters $a = 3.2540$ Å, $c = 5.2150$ Å, $c/a = 1.603$ for ZnO NPs (100°C) and $a = 3.2490$ Å, $c = 5.2050$ Å, $c/a = 1.605$ for ZnO NPs (550°C), which matches the hexagonal wurtzite structure of ZnO NPs. Hexagonal wurtzite structure of ZnO is the most stable phase of ZnO [25]. Diffraction peaks of other impurities such as $Zn(OH)_2$ or constituents of *C. sativum* leaf extract were not detected, indicating that relatively pure ZnO was

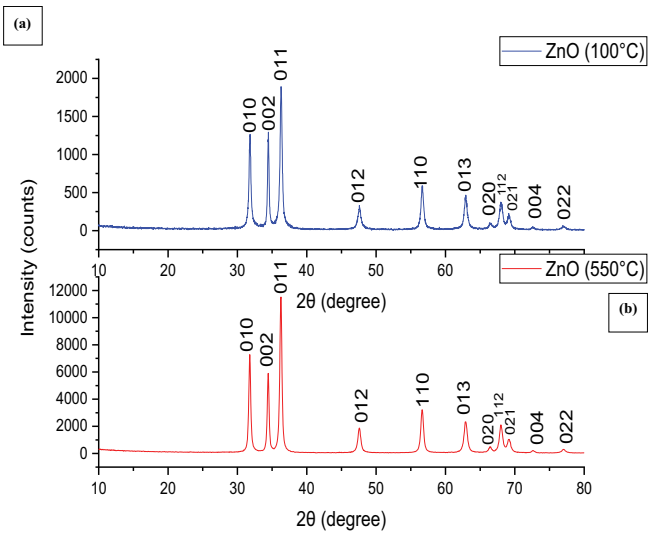

Fig. 9. XRD patterns of ZnO NPs (100°C) and ZnO NPs (550°C).

obtained. The result proves that the peaks observed in the XRD spectrum belonged only to ZnO. The broadening of the peaks in XRD indicates the formation of nanosized particles [12]. The XRD peaks are broader as the NPs size decreases [55]. The average particle size of ZnO NPs was calculated from the three most intense peaks using Debye–Scherrer's formula, which gives a relationship between particle size and the peak broadening in XRD:

$$D = \frac{K\lambda}{\beta\cos\theta} \tag{2}$$

where D is crystal particle size, K is Scherrer's constant (0.9), λ is the wavelength of X-ray (0.15406 nm), β is the full width at half maximum (FWHM) of the intensity peaks, and θ is the Bragg's diffraction angle. Utilising the Scherrer formula, the average crystalline sizes of ZnO NPs (100°C) and ZnO NPs (550°C) were determined to be 60.85 and 55.13 nm, respectively.

3.7. Fourier transform infrared spectroscopy analysis

The FTIR spectrum of ZnO NPs was analysed in the range of 4,000 to 400 cm^{-1} (Fig. 10) to detect the possible biomolecules or functional groups involved in the green synthesis procedure for the reduction of Zn^{2+} ions that leads to the stability of NPs. Metal oxides generally exhibit absorption bands in the fingerprint region (below 1,000 cm^{-1}). This might be due to inter-nuclear vibrations [6]. For ZnO NPs (100°C), the peaks were detected at 1,566.19 and 1,412.07 cm^{-1}, and at 1,406 cm^{-1} for ZnO NPs (550°C). These peaks are assigned to C–O, =C–H, C=C, and –C–O–C stretching modes from the protein. These findings show that proteins can bind to ZnO NPs through the available amine groups or residues in the proteins. The band which appeared at 3,307.01 and 3,394.25 cm^{-1} for ZnO NPs (100°C) and ZnO NPs (550°C), respectively, might be due to asymmetric and symmetric stretching hydrogen bond OH of alcohol or phenolic compound [2]. Similarly, Sasirekha et al. [56] reported that bulk

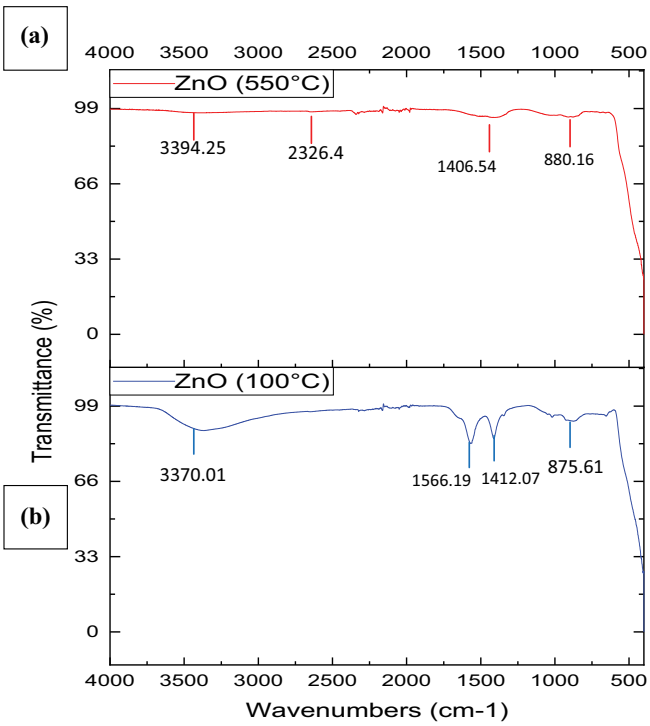

Fig. 10. FTIR spectrum of ZnO NPs (100°C) and ZnO NPs (550°C).

ZnO synthesised from leaf extracts of *Plectranthus barbatus* showed a high intensity broad band around 3,429 cm^{-1}. The weaker band at 875.61 and 880.16 cm^{-1} for ZnO NPs (100°C) and ZnO NPs (550°C), respectively, corresponds to amide I, arising due to the carbonyl stretch in proteins. The IR spectra prove that the ZnO absorption band with stretching mode of Zn–O was between 500 and 600 cm^{-1} [25]. Hence, the region between 500 and 600 cm^{-1} is attributed to Zn–O group [43]. Consequently, the synthesised ZnO NPs were encompassed by proteins and metabolites, for example, terpenoids, a polyphenolic functional groups. The FTIR studies confirmed that the natural biological moieties could perform dual functions in the formation and stabilisation of synthesised ZnO NPs in the aqueous medium [57,58]. Fowsiya et al. [59] observed a region in the lower energy at 428 cm^{-1} of the FTIR spectrum of ZnO NPs synthesised from *Carissa edulis* extract and attributed it to the ZnO bond bending vibration.

The utilization of environmentally benign plant extract makes the ZnO NPs have promising potential applications in catalysis, opto-electronics, gas sensing [60], agricultural [11], electrochemical sensor [61], biomedical [37], and medical devices [62].

4. Conclusion

ZnO NPs were successfully synthesised via green synthesis method using *C. sativum* leaf extract. The green synthesis method using *C. sativum* leaf extract as a stabilisers/reducing agent in the current work was effective in stabilising the ZnO NPs. Moreover, an increase in calcination temperature for the synthesis of ZnO NPs resulted in better structural properties such as smaller nanosized particle and better crystalline phase from XRD analysis. From the XRD analysis, the

average crystalline size of ZnO NPs was between 55.13 and 60.85 nm. Moreover, SEM and TEM analysis showed that the ZnO NPs can be clearly distinguished as individual particles with no agglomeration.

Acknowledgements

The authors would like to thank the Research Management Centre (RMC), UTHM for providing GPPS Grant (H017) and Tier 1 Grant (H207) and FRGS vot K090 as a financial support for this research.

References

[1] M.A. Gatoo, S. Naseem, M.Y. Arfat, A.M. Dar, K. Qasim, S. Zubair, Physicochemical properties of nanomaterials implication in associated toxic manifestations, BioMed Res. Int., 2014 (2014) 8.
[2] N. Senthilkumar, V. Aravindhan, K. Ruckmani, I.V. Potheher, *Coriandrum sativum* mediated synthesis of silver nanoparticles and evaluation of their biological characteristics, Mater. Res. Express, 5 (2018) 055032.
[3] N. Matinise, X.G. Fuku, K. Kaviyarasu, N. Mayedwa, M. Maaza, ZnO nanoparticles via *Moringa oleifera* green synthesis: physical properties & mechanism of formation, Appl. Surf. Sci., 406 (2017) 339–347.
[4] M.Z.H. Khan, F.K. Tareq, M.A. Hossen, M.N.A.M. Roki, Green synthesis and characterization of silver nanoparticles using Coriandrum sativum leaf extract, J. Eng. Sci. Technol., 13 (2018) 158–166.
[5] J. Virkutyte, R.S. Varma, Green Synthesis of Nanomaterials: Environmental Aspects, Sustainable Nanotechnology and the Environment Advances and Achievements, ACS Symposium Series, American Chemical Society, 2013, pp. 11–39.
[6] A. Raja, S. Ashokkumar, R.P. Marthandam, J. Jayachandiran, C.P. Kathiwada, K. Kaviyarasu, R.G. Raman, M. Swaminathan, Eco-friendly preparation of zinc oxide nanoparticles using *Tabernaemontana divaricata* and its photocatalytic and antimicrobial activity, J. Photochem. Photobiol. B Biol., 181 (2018) 53–58.
[7] D. Gnanasangeetha, D. Saralathambavani, One Pot synthesis of zinc oxide nanoparticles via chemical and green method, Res. J. Mater. Sci., 1 (2013) 1–8.
[8] H. Agarwal, S. Venkat Kumar, S. Rajeshkumar, A review on green synthesis of zinc oxide nanoparticles – an eco-friendly approach, Resour. Technol., 3 (2017) 406–413.
[9] A. Kołodziejczak-radzimska, T. Jesionowski, Zinc oxide—from synthesis to application: a review, Mater. (Basel, Switzerland), 7 (2014) 2833–2881.
[10] M. Bordbar, N. Negahdar, M. Nasrollahzadeh, *Melissa Officinalis* L. leaf extract assisted green synthesis of CuO/ZnO nanocomposite for the reduction of 4-nitrophenol and Rhodamine B, Sep. Purif. Technol., 191 (2018) 295–300.
[11] S. Sabir, M. Arshad, S.K. Chaudhari, Zinc oxide nanoparticles for revolutionizing agriculture, Sci. World J., 2014 (2014) 1–8.
[12] K.B. Narayanan, N. Sakthivel, Coriander leaf mediated biosynthesis of gold nanoparticles, Mater. Lett., 62 (2008) 4588–4590.
[13] R. Amooaghaie, M.R. Saeri, M. Azizi, Synthesis, characterization and biocompatibility of silver nanoparticles synthesized from *Nigella sativa* leaf extract in comparison with chemical silver nanoparticles, Ecotoxicol. Environ. Saf., 120 (2015) 400–408.
[14] D. Suresh, P.C. Nethravathi, Udayabhanu, H. Rajanaika, H. Nagabhushana, S.C. Sharma, Green synthesis of multifunctional zinc oxide (ZnO) nanoparticles using *Cassia fistula* plant extract and their photodegradative, antioxidant and antibacterial activities, Mater. Sci. Semicond. Process., 31 (2015) 446–454.
[15] K. Elumalai, S. Velmurugan, S. Ravi, V. Kathiravan, S. Ashokkumar, Green synthesis of zinc oxide nanoparticles using *Moringa oleifera* leaf extract and evaluation of its antimicrobial activity, Spectrochim. Acta - Part A Mol. Biomol. Spectrosc., 143 (2015) 158–164.
[16] S. Vijayakumar, B. Vaseeharan, B. Malaikozhundan, M. Shobiya, *Laurus nobilis* leaf extract mediated green synthesis of ZnO nanoparticles: characterization and biomedical applications, Biomed. Pharmacother., 84 (2016) 1213–1222.
[17] P. Mishra, Y.P. Singh, H.P. Nagaswarupa, S.C. Sharma, Y.S. Vidya, S.C. Prashantha, H. Nagabhushana, K.S. Anantharaju, S. Sharma, L. Renuka, *Caralluma fimbriata* extract induced green synthesis, structural, optical and photocatalytic properties of ZnO nanostructure modified with Gd, J. Alloys Compd., 685 (2016) 656–669.
[18] Udayabhanu, G. Nagaraju, H. Nagabhushana, D. Suresh, C. Anupama, G.K. Raghu, S.C. Sharma, *Vitis labruska* skin extract assisted green synthesis of ZnO super structures for multifunctional applications, Ceram. Int., 43 (2017) 11656–11667.
[19] C. Vidya, C. Manjunatha, M.N. Chandraprabha, M. Rajshekar, M.A.L. Antony Raj, Hazard free green synthesis of ZnO nano-photo-catalyst using Artocarpus Heterophyllus leaf extract for the degradation of Congo red dye in water treatment applications, J. Environ. Chem. Eng., 5 (2017) 3172–3180.
[20] K. Steffy, G. Shanthi, A.S. Maroky, S. Selvakumar, Enhanced antibacterial effects of green synthesized ZnO NPs using *Aristolochia indica* against Multi-drug resistant bacterial pathogens from diabetic foot ulcer, J. Infect. Public Health. Health, 11 (2018) 463–471.
[21] D. Sharma, M.I. Sabela, S. Kanchi, K. Bisetty, A.A. Skelton, B. Honarparvar, Green synthesis, characterization and electrochemical sensing of silymarin by ZnO nanoparticles: experimental and DFT studies, J. Electroanal. Chem., 808 (2018) 160–172.
[22] V. Prachayasittikul, S. Prachayasittikul, S. Ruchirawat, V. Prachayasittikul, Coriander (*Coriandrum sativum*): a promising functional food toward the well-being, Food Res. Int., 105 (2018) 305–323.
[23] M. Ovais, A.T. Khalil, N.U. Islam, I. Ahmad, M. Ayaz, Role of plant phytochemicals and microbial enzymes in biosynthesis of metallic nanoparticles, Appl. Microbiol Biotechnol., 102 (2018) 6799–6814.
[24] R. Sathyavathi, M.B. Krishna, S.V. Rao, R. Saritha, D. Narayana Rao, Biosynthesis of silver nanoparticles using *Coriandrum sativum* leaf extract and their application in nonlinear optics, Adv. Sci. Lett., 3 (2010) 138–143.
[25] G.M. Nazeruddin, N.R. Prasad, S.R. Prasad, Y.I. Shaikh, S.R. Waghmare, P. Adhyapak, Coriandrum sativum seed extract assisted in situ green synthesis of silver nanoparticle and its anti-microbial activity, Ind. Crops Prod., 60 (2014) 212–216.
[26] S.S.M. Hassan, W.I.M. El Azab, H.R. Ali, M.S.M. Mansour, Green synthesis and characterization of ZnO nanoparticles for photocatalytic degradation of anthracene, Adv. Nat. Sci. Nanosci. Nanotechnol., 6 (2015) 045012.
[27] S. Pratap Goutam, A. Kumar Yadav, A. Jyoti Das, Coriander extract mediated green synthesis of zinc oxide nanoparticles and their structural, optical and antibacterial, J. Nanosci. Technol., 3 (2017) 249–252.
[28] J. Singh, S. Kaur, G. Kaur, S. Basu, M. Rawat, Biogenic ZnO nanoparticles: A study of blueshift of optical band gap and photocatalytic degradation of reactive yellow 186 dye under direct sunlight, Green Process. Synth., 8 (2019) 272–280.
[29] G. Sharmila, M. Thirumarimurugan, C. Muthukumaran, Green synthesis of ZnO nanoparticles using *Tecoma castanifolia* leaf extract: characterization and evaluation of its antioxidant, bactericidal and anticancer activities, Microchem. J., 145 (2019) 578–587.
[30] S.A. Khan, F. Noreen, S. Kanwal, A. Iqbal, G. Hussain, Green synthesis of ZnO and Cu-doped ZnO nanoparticles from leaf extracts of *Abutilon indicum*, *Clerodendrum infortunatum*, *Clerodendrum inerme* and investigation of their biological and photocatalytic activities, Mater. Sci. Eng. C, 82 (2018) 46–59.
[31] T. Karnan, S.A.S. Selvakumar, Biosynthesis of ZnO nanoparticles using rambutan (*Nephelium lappaceum* L.) peel extract and their photocatalytic activity on methyl orange dye, J. Mol. Struct., 1125 (2016) 358–365.

[32] B. Stevens, S. Bell, K. Adams, Initial evaluation of inlet thermal desorption GC – MS analysis for organic gunshot residue collected from the hands of known shooters, Forensic Chem., 2 (2016) 55–62.
[33] B. Archana, K. Manjunath, G. Nagaraju, K.B. Chandra Sekhar, N. Kottam, Enhanced photocatalytic hydrogen generation and photostability of ZnO nanoparticles obtained via green synthesis, Int. J. Hydrogen Energy, 42 (2017) 5125–5131.
[34] H. Bozetine, Q. Wang, A. Barras, M. Li, T. Hadjersi, S. Szunerits, R. Boukherroub, Green chemistry approach for the synthesis of ZnO-carbon dots nanocomposites with good photocatalytic properties under visible light, J. Colloid Interface Sci., 465 (2016) 286–294.
[35] W. Da Oh, L.W. Lok, A. Veksha, A. Giannis, T.T. Lim, Enhanced photocatalytic degradation of bisphenol A with Ag-decorated S-doped g-C_3N_4under solar irradiation: performance and mechanistic studies, Chem. Eng. J., 333 (2018) 739–749.
[36] S.B. Reddy, B.K. Mandal, Facile green synthesis of zinc oxide nanoparticles by *Eucalyptus globulus* and their photocatalytic and antioxidant activity, Adv. Powder Technol., 28 (2017) 785–797.
[37] S.S. Momeni, M. Nasrollahzadeh, A. Rustaiyan, Green synthesis of the Cu/ZnO nanoparticles mediated by *Euphorbia prolifera* leaf extract and investigation of their catalytic activity, J. Colloid Interface Sci., 472 (2016) 173–179.
[38] M. Nasrollahzadeh, S.M. Sajadi, M. Maham, Green synthesis of palladium nanoparticles using *Hippophae rhamnoides* Linn leaf extract and their catalytic activity for the Suzuki – Miyaura coupling in water, J. Mol. Catal. A, Chem., 396 (2015) 297–303.
[39] M. Atarod, M. Nasrollahzadeh, S.M. Sajadi, *Euphorbia heterophylla* leaf extract mediated green synthesis of Ag/TiO_2 nanocomposite and investigation of its excellent catalytic activity for reduction of variety of dyes in water, J. Colloid Interface Sci., 462 (2016) 272–279.
[40] D. Suresh, P.C. Nethravathi, Udayabhanu, M.A. Pavan Kumar, H. Raja Naika, H. Nagabhushana, S.C. Sharma, Chironji mediated facile green synthesis of ZnO nanoparticles and their photoluminescence, photodegradative, antimicrobial and antioxidant activities, Mater. Sci. Semicond. Process., 40 (2015) 759–765.
[41] P.C. Nagajyothi, S. Ju, I. Jun, T.V.M. Sreekanth, K. Joong, H. Mook, Antioxidant and anti-inflammatory activities of zinc oxide nanoparticles synthesized using *Polygala tenuifolia* root extract, J. Photochem. Photobiol. B Biol., 146 (2015) 10–17.
[42] H.H.R. Madan, S.C. Sharma, Udayabhanu, D. Suresh, Y.S. Vidya, P.S. Nagabhushana, H. Rajanaik, K.S. Anantharaju, S.C. Prashantha, Maiya, Facile green fabrication of nanostructure ZnO plates, bullets, flower, prismatic tip, closed pine cone: their antibacterial, antioxidant, photoluminescent and photocatalytic properties, Spectrochim. ACTA PART A Mol. Biomol. Spectrosc., (2015). doi:10.1016/j.saa.2015.07.067.
[43] B. Malaikozhundan, J. Vinodhini, Nanopesticidal effects of *Pongamia pinnata* leaf extract coated zinc oxide nanoparticle against the Pulse beetle, *Callosobruchus maculatus*, Mater. Today Commun., 14 (2018) 106–115.
[44] S. Vijayakumar, G. Vinoj, B. Malaikozhundan, S. Shanthi, B. Vaseeharan, *Plectranthus amboinicus* leaf extract mediated synthesis of zinc oxide nanoparticles and its control of methicillin resistant *Staphylococcus aureus* biofilm and blood sucking mosquito larvae, Spectrochim. Acta - Part A Mol. Biomol. Spectrosc., 137 (2015) 886–891.
[45] A. Gupta, P. Srivastava, L. Bahadur, D.P. Amalnerkar, R. Chauhan, Comparison of physical and electrochemical properties of ZnO prepared via different surfactant-assisted precipitation routes, Appl. Nanosci., 5 (2015) 787–794.
[46] V. Sai Saraswathi, J. Tatsugi, P.K. Shin, K. Santhakumar, Facile biosynthesis, characterization, and solar assisted photocatalytic effect of ZnO nanoparticles mediated by leaves of L. speciosa, J. Photochem. Photobiol. B Biol., 167 (2017) 89–98.
[47] M. Ramesh, M. Anbuvannan, G. Viruthagiri, Green synthesis of ZnO nanoparticles using *Solanum nigrum* leaf extract and their antibacterial activity, Spectrochim. Acta - Part A Mol. Biomol. Spectrosc., 136 (2014) 864–870.
[48] S. Karthik, P. Siva, K.S. Balu, R. Suriyaprabha, V. Rajendran, M. Maaza, *Acalypha indica*–mediated green synthesis of ZnO nanostructures under differential thermal treatment: effect on textile coating, hydrophobicity, UV resistance, and antibacterial activity, Adv. Powder Technol., 28 (2017) 3184–3194.
[49] M. Sundrarajan, S. Ambika, K. Bharathi, Plant-extract mediated synthesis of ZnO nanoparticles using *Pongamia pinnata* and their activity against pathogenic bacteria, Adv. Powder Technol., 26 (2015) 1294–1299.
[50] B. Malaikozhundan, B. Vaseeharan, S. Vijayakumar, K. Pandiselvi, M.A.R. Kalanjiam, K. Murugan, G. Benelli, Biological therapeutics of *Pongamia pinnata* coated zinc oxide nanoparticles against clinically important pathogenic bacteria, fungi and MCF-7 breast cancer cells, Microb. Pathog., 104 (2017) 268–277.
[51] C. Vidya, M.N.C. Prabha, M.A.L.A. Raj, Green mediated synthesis of zinc oxide nanoparticles for the photocatalytic degradation of Rose Bengal dye, Environ. Nanotechnology, Monit. Manage., 6 (2016) 134–138.
[52] M.S. Geetha, H. Nagabhushana, H.N. Shivananjaiah, Green mediated synthesis and characterization of ZnO nanoparticles using *Euphorbia Jatropa* latex as reducing agent, J. Sci. Adv. Mater. Devices, 1 (2016) 301–310.
[53] R. Ishwarya, B. Vaseeharan, S. Kalyani, B. Banumathi, M. Govindarajan, N.S. Alharbi, S. Kadaikunnan, M.N. Al-anbr, J.M. Khaled, G. Benelli, Facile green synthesis of zinc oxide nanoparticles using *Ulva lactuca* seaweed extract and evaluation of their photocatalytic, antibiofilm and insecticidal activity, J. Photochem. Photobiol. B Biol., 178 (2018) 249–258.
[54] F.T. Thema, E. Manikandan, M.S. Dhlamini, M. Maaza, Green synthesis of ZnO nanoparticles via *Agathosma betulina* natural extract, Mater. Lett., 161 (2015) 124–127.
[55] S. Vijayakumar, B. Vaseeharan, B. Malaikozhundan, M. Divya, M. Abhinaya, N. Gobi, A. Bhattacharyya, N. Balashanmugam, D. Surmistha, K. Murugan, G. Benelli, Ecotoxicity of *Musa paradisiaca* leaf extract-coated ZnO nanoparticles to the freshwater microcrustacean *Ceriodaphnia cornuta*, Limnologica, 67 (2017) 1–6.
[56] C. Sasirekha, S. Arumugam, G. Muralidharan, Green synthesis of ZnO/carbon (ZnO/C) as an electrode material for symmetric supercapacitor devices, Appl. Surf. Sci., 449 (2018) 521–527.
[57] M. Noruzi, Biosynthesis of gold nanoparticles using plant extracts, Bioprocess Biosyst. Eng., 38 (2015) 1–14.
[58] S. Vijayakumar, B. Malaikozhundan, S. Shanthi, B. Vaseeharan, N. Thajuddin, Control of biofilm forming clinically important bacteria by green synthesized ZnO nanoparticles and its ecotoxicity on *Ceriodaphnia cornuta*, Microb. Pathog., 107 (2017) 88–97.
[59] J. Fowsiya, G. Madhumitha, N.A. Al-dhabi, M. Valan, Photocatalytic degradation of Congo red using *Carissa edulis* extract capped zinc oxide nanoparticles, J. Photochem. Photobiol., B, 162 (2016) 395–401.
[60] C.B. Ong, L.Y. Ng, A.W. Mohammad, A review of ZnO nanoparticles as solar photocatalysts: synthesis, mechanisms and applications, Renew. Sustain. Energy Rev., 81 (2018) 536–551.
[61] N.S. Pavithra, K. Lingaraju, G.K. Raghu, G. Nagaraju, *Citrus maxima* (Pomelo) juice mediated eco-friendly synthesis of ZnO nanoparticles: applications to photocatalytic, electrochemical sensor and antibacterial activities, Spectrochim. Acta - Part A Mol. Biomol. Spectrosc., 185 (2017) 11–19.
[62] H.S. Lalithamba, M. Raghavendra, K. Uma, K.V. Yatish, D. Mousumi, G. Nagendra, *Capsicum annuum* fruit extract : a novel reducing agent for the green synthesis of ZnO nanoparticles and their multifunctional applications, Acta Chim. Sloven., 65 (2018) 354–364.